

Non-conservative forces and effective temperatures in active polymers

Davide Loi,¹ Stefano Mossa,^{2,*} and Leticia F. Cugliandolo^{3,†}

¹ *European Synchrotron Radiation Facility, BP 220, F-38043 Grenoble France*

² *UMR 5819 (UJF, CNRS, CEA) CEA, INAC, SPrAM,*

17 Rue des Martyrs, 38054 Grenoble Cedex 9, France

³ *Université Pierre et Marie Curie – Paris VI, LPTHE UMR 7589, 4 Place Jussieu, 75252 Paris Cedex 05, France*

(Dated: October 26, 2018)

We follow the dynamics of an ensemble of interacting self-propelled semi-flexible polymers in contact with a thermal bath. We characterize structure and dynamics of the passive system and as a function of the motor activity. We find that the fluctuation-dissipation relation allows for the definition of an effective temperature that is compatible with the results obtained by using a tracer particle as a thermometer. The effective temperature takes a higher value than the temperature of the bath when the effect of the motors is not correlated with the structural rearrangements they induce. Our data are compatible with a dependence upon the square of the motor strength (normalized by the average internal force) and they suggest an intriguing linear dependence on the tracer diffusion constant times the density of the embedding matrix. We show how to use this concept to rationalize experimental results and suggest possible innovative research directions.

I. INTRODUCTION

The constituents of active matter, be them particles, lines or other, absorb energy from their environment or internal fuel tanks and use it to carry out motion. In this new type of soft condensed matter energy is partially transformed into mechanical work and partially dissipated in the form of heat [1]. The units interact directly or through disturbances propagated in the medium.

In systems of biological interest, conservative forces (and thermal fluctuations) are complemented by non-conservative forces. Realizations of active matter in biology are thus manifold and exist at different scales. Some of them are: bacterial suspensions [2–5], the cytoskeleton in living cells [6–10], or even swarms of different animals [11].

Clearly enough, active matter is far from equilibrium and typically kept in a non-equilibrium steady state. The difference between active matter and other driven systems, such as sheared fluids, vibrated granular matter and driven vortex lattices is that the energy input is located on internal units (*e.g.* motors) and therefore homogeneously distributed in the sample. In the other driven systems just mentioned, the energy input occurs on the boundaries of the sample. Moreover, the effect of the motors can be dictated by the state of the particle and/or its immediate neighborhood and it is not necessarily fixed by an external field.

The dynamics of active matter presents a number of interesting features that are worth mentioning here. Active matter displays out of equilibrium phase transitions that may be absent in their passive counterparts. The dynamic states display large scale spatio-temporal dynamical patterns and depend upon the energy flux and the

interactions between their constituents. Active matter often exhibits unusual mechanical properties, very large responses to small perturbations, and very large fluctuations – not consistent with the central limit theorem.

Much theoretical effort has been recently devoted to the description of different aspects of these systems. The investigation of the self-organization of living microorganisms is summarized in [12]. The identification and analysis of states with spatial structure, such as bundles, vortices and asters was developed in, *e.g.*, [13–15]. The study of the rheological properties of active particle suspensions was carried out in [16–19] with the aim of grasping which are the mechanical consequences of biological activity.

Surprisingly enough, molecular dynamics computer simulations, that have proven to be so helpful to probe and understand the dynamics of complex passive systems, have not been much employed in the field of active matter yet. (For a recent review of the most used computational approaches to cell mechanics see Ref. [20].) Studies presented so far have been mainly analytical, based on refined calculations on very stylized models [3, 4, 11–18], computer simulations of continuum models, *e.g.*, Lattice Boltzmann equations [21], and numerical studies of relatively simple lattice models as the ones pioneered by Vicsek and collaborators [4, 5, 22, 23].

Quite independently, passive systems with complex out of equilibrium dynamics have been the focus of much attention too. These are systems with competing interactions between their constituents – and no external energy input – that in some conditions – such as sufficiently low temperature or high density – cannot equilibrate with their environment. A regime (or phase) with glassy properties then occurs. In the last two decades or so, a rather complete mean-field theory that describes, up to a certain extent, the super-cooled liquid and deep glassy regime, developed [24–28]. Keywords are “mode-coupling theory” and the “random first order phase transition scenario”. This has been complemented with ex-

*stefano.mossa@cea.fr

†leticia@lpthe.jussieu.fr

tensive molecular dynamic simulations of microscopic models with interactions between their constituents that are as realistic as possible [27, 28]. Simulations have shown agreement with certain aspects of the theoretical approach, especially the ones that will be of interest in this paper.

An important outcome of such theoretical modeling of glassy systems, later confirmed with numerical simulations, is the generation of an effective temperature, T_{eff} , in super-cooled liquids driven out of equilibrium and glasses in relaxation [29, 30]. The concept of effective temperatures in out of equilibrium systems, as arising from deviations from the fluctuation-dissipation theorem (FDT) [31], appeared in studies of dynamical systems [32] and it was later extended and developed in the field of glassy systems [29]. It was here fully appreciated that T_{eff} should be understood as a time-scales dependent parameter and that it takes a thermodynamic meaning in systems with slow dynamics only [29, 33]. It was later proven that in systems with sufficiently slow dynamics – reaching a regime of small entropy production – the same values of the effective temperature are obtained with a variety of other measurements. Experimental measurements of T_{eff} in different glassy systems, including glycerol [34], spin-glasses [35], polymer samples [36], granular matter [37, 38], laponite [39] and other colloidal suspensions [40] have been performed. Very recently, a study of T_{eff} in an active colloidal suspension of Janus particles under a gravity field appeared in [41] and we shall comment on this work later in the context of our results. On the numerical side, the work in [42] is especially relevant to our study and we shall also comment on it below. The validity of FDT in the Vicsek model was investigated in [5, 22]. In the latter paper a dynamic measurement, similar to one of the calculations we present below, was performed.

In [43] we took a first step in the direction of analyzing the structure and dynamics of active matter with molecular dynamics numerical methods. We studied the dynamics of an ensemble of self-propelled particles in contact with an equilibrated thermal bath, a reasonable model for real but simple active matter, such as bacterial colonies. In particular, we analyzed the generation of an effective temperature and some of its properties. In this article we go beyond this study to get closer to more complex cases. We introduce a model for biological structures made of filamentous semi-flexible polymers [44]. We analyze its structure and dynamics and we study the effective temperature by using a variety of independent measurements. In particular, we show how to measure the effective temperature by using techniques that have already been exploited in the study of the mechanical properties of real biological systems. The idea is to mimic real experiments which probe mechanical properties of the embedding matrix by following the dynamics of tracer particles (see, among many others, Refs. [45–47]), both free and driven by external fields, *e.g.*, optical tweezers. We demonstrate that these techniques can be useful to obtain

a direct characterization of the out-of-equilibrium state, and allow for the determination of an effective temperature. A short summary of some of the results included in the present work can be found in Ref. [48].

The paper is organized as follows. In Section II we give details of the model and the molecular dynamics computer simulations performed. Section III presents a study of the molecular model in its passive limit in which we determine the optimal parameters, in particular the polymer length, to be used in the simulations of the active case. In Section IV we describe our results on the structure and dynamics of the molecular active matter model. Section V contains a detailed analysis of the effective temperature measured by different methods and a comparison with other studies in the literature. Our entire set of data is discussed and put in more perspective in Section VI, where we also give some conclusions and a few hints for future work.

II. MODEL AND METHODS

Many complex biological systems are constituted of elongated fibrillar structures (filaments) [44]. Although one could expect to use the well-established polymer theory to describe such systems, this theory focuses on the limits of completely flexible or totally rigid polymers [49, 50] and most biologically relevant polymers or filaments are in neither of these classes. They rather belong in a third intermediate category: the one of semi-flexible filaments with persistence and contour lengths [51] of comparable magnitude. The contour length of these filaments is too small for them to form loops and knots, yet they are sufficiently flexible to have significant thermal bending. These problems are much harder to deal with analytically [52] and, surprisingly enough, relatively little numerical work has been done so far. In this paper we start filling this gap by presenting molecular dynamics simulations of a simple but sufficiently realistic model mimicking the behavior of semi-flexible (or semi-rigid) polymers in interaction.

A. Semi-flexible polymer model

We consider a model of a (passive) semi-flexible polymer in which the components have the shape of filaments. Each filament is a linear chain of beads. The optimal values of the parameters have been fixed by preliminary calculations, detailed in [53]. We briefly motivate them here.

Polymer chains are coarse-grained and each segment is formed by a bead. Each bead is in contact with a thermal environment that is described by a random noise and a viscous drag. The i th monomer pertaining to chain labeled a has coordinates \mathbf{r}_{ia} and velocity \mathbf{v}_{ia} . The latter evolve following the Langevin equation:

$$m_i \dot{\mathbf{v}}_{ia} = -\xi m_{ia} \mathbf{v}_{ia} + \mathbf{f}_{ia}^s + \mathbf{f}_{ia}^M + \boldsymbol{\eta}_{ia}. \quad (1)$$

$\boldsymbol{\eta}_{ia}$ is a Gaussian white noise representing thermal agitation with zero mean and variance $\langle \eta_{ia}^\mu(t) \eta_{jb}^\nu(t') \rangle = 2\xi m_{ia} T \delta(t-t') \delta^{\mu\nu} \delta_{ij} \delta_{ab}$, where $\mu, \nu = 1, \dots, d$ and d is the dimension of space ($d = 3$ in what follows). The temperature of the bath is T and we set $k_B = 1$ henceforth. The term $-\xi m_{ia} \mathbf{v}_{ia}$ is the frictional force. We take into account the over-damped character of the dynamics by considering a large value of the friction coefficient. The numerical integration of Eq. (1) generates a time evolution that is consistent with the canonic ensemble (NVT) in thermodynamic equilibrium. Note that we completely disregard the effect of hydrodynamic interactions due to internal and/or intermolecular degrees of freedom. We consider identical beads, with masses $m_{ia} = m$ and diameter $r_{ia} = r_0$ for all i and a .

The deterministic mechanical conservative force on monomer i pertaining to polymer a due to all other components is $\mathbf{f}_{ia}^s \equiv \sum_{b=1}^{N_p} \sum_{j=1}^{N_m} \mathbf{f}_{ijab}^s =$

$-\sum_{b=1}^{N_p} \sum_{j=1}^{N_m} \nabla_{ia} U_{tot}(r_{ij}^{ab})$, where r_{ij}^{ab} is the distance between monomer i in polymer a and monomer j in polymer b . N_m and N_p are the total number of monomers per chain and the total number of polymers respectively. All polymers have the same length N_m . We consider the interaction potential

$$U_{tot}(r) = U_{intra}(r) + U_{inter}(r), \quad (2)$$

in which the two terms are the intramolecular ($a \neq b$) and intermolecular ($a = b$) contributions, respectively. The exact form of the two contributions must be chosen in order to expand the region of stability of the liquid state, avoiding crystallization, and to tune the degree of flexibility of the polymer chains, thus inhibiting complete folding of the chains.

For the intermolecular interactions we choose

$$U_{inter}(r_{ij}) = \left\{ 4\epsilon \left[\left(\frac{\sigma}{r_{ij}} \right)^{12} - \left(\frac{\sigma}{r_{ij}} \right)^6 \right] - U(r_c) \right\} \theta(r_c - r), \quad (3)$$

i.e., the usual Lennard-Jones interaction potential cut and shifted to zero at r_c by adding the constant value $-U(r_c)$. In addition, we consider $r_c = 2^{1/6}\sigma$, corresponding to the position of the minimum of the pure Lennard-Jones potential, and obtain a purely repulsive potential ($U(r_c) = -\epsilon$ in this case). The Heaviside function θ assures that the potential is zero for $r > r_c$. This par-

ticular choice is done to obtain a polymer density in the melting state lower than the one achieved by considering attractive interactions, thus avoiding crystallization at low temperatures [53]. ϵ has energy units and controls the strength of the interaction. σ has length units and fixes the typical length scale of the system.

The intramolecular potential reads:

$$U_{intra}(r_{ij}) = \begin{cases} k(r_{ij} - r_0)^2, & \text{if } i, j \text{ n.n.} \\ \left\{ 4\epsilon \left[\left(\frac{S}{r_{ij}} \right)^{12} - \left(\frac{S}{r_{ij}} \right)^6 \right] - U(r_c) \right\} \theta(r_c - r), & \text{if } i, j \text{ n.n.n.} \end{cases} \quad (4)$$

Connectivity of the chain is assured by harmonic springs of elastic constant k and equilibrium length r_0 , acting between nearest neighbor monomers. Chain rigidity is controlled by a repulsive Lennard Jones potential between next nearest neighbors, with $r_c = 2^{1/6}S$ and again $U(r_c) = -\epsilon$. Finally, monomers separated by more than two bonds interact via Eq. (3). The actual choice for the parameters k , r_0 and S allows one to control the flexibility of the chains, ranging from semi-rigid to flexible chains [53]. In particular, it is evident that chain rigidity can be induced by a mismatch of the zero point energy position of the two terms in Eq. (4) taken separately. Therefore, the relevant parameter is the ratio

r_0/S . Miura *et al.* [53] found that the average cosine of the angle between two successive bond vectors along the chain equals 0.92, *i.e.*, the chain is semi-rigid, for $S \simeq 2.5r_0$.

B. The molecular motors

A preliminary remark about the implementation of realistic molecular motors in a coarse-grained computer simulation study is obvious: no simple technique is able to take into account chemical activity in a molecular dynamics calculation. Having this in mind, particular care

and physical insight has been put in the choice of a reasonable model for motor action on a particular monomer, say the i th in the a th chain, that we call \mathbf{f}_{ia}^M . Only a fixed fraction of polymers are provided with motors. This choice is mainly due to the requirements that motor activity: i) should be homogeneously distributed in the sample; ii) should have a gentle but still detectable out-of-equilibrium effect on the behavior of the system; iii) should stay in the linear response regime.

Following symmetry considerations, we chose to localize the non-conservative polymer activity at the core of the filament, *i.e.*, we motorized the very central monomer in the polymer only. Note that, in general, this position does not coincide with the center of mass of the filament and, most importantly, it is fixed. This situation is clearly at variance with the case of real systems, where molecular motors are able to slide along the filaments [6]. Nevertheless, we do not consider this a serious limitation to our approach, since we follow the dynamical behavior of the system on limited time scales over which motor activity can be indeed taken as localized. Also, we average our results over a substantial number of different instances of motor realizations, mimicking in an indirect way motor motion relative to the filaments. A typical isolated flexible polymer configuration studied is shown in Fig. 1.

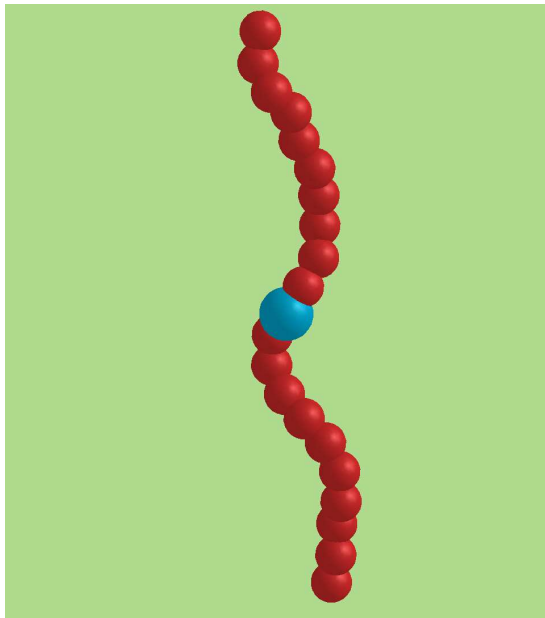


FIG. 1: The semi-flexible polymer model considered in this paper. It is formed by 21 monomers among which 20 are non-motorized (red spheres). The entire chemical motor activity is localized on the central monomer (blue sphere). Although all monomers have the same size we draw a larger central monomer in the sketch to emphasize its particular role.

Similar to the case of self-propelled spherical particles [43], we mimic the motor effect with a time series of random isotropic kicks, generated by a suitable stochas-

tic process controlled by three parameters: i) the number of motorized polymers; ii) the intensity and direction of the motors forces; and iii) the activation time scale. During τ steps of the molecular dynamics trajectory, independent forces are applied to a fraction of randomly chosen motorized central monomers. The strength of the force exerted, $f^M = |\mathbf{f}_{ia}^M|$ is the same for all motors and is chosen to be a fraction of the mean conservative mechanical force acting on the equivalent passive system, $\bar{F} = (N_p N_m)^{-1} \sum_{a=1}^{N_p} \sum_{i=1}^{N_m} |\mathbf{f}_{ia}^s|$. We quantify the motor activity with the control parameter $f = f^M / \bar{F}$. The direction of the motor force is chosen at random isotropically, to avoid preferential flows in the system. The subset of propelled monomers and the directions of the applied forces change at each power stroke of duration τ . In short, we focus on *adamant* [54] motors, *i.e.* their action is completely independent of the structural rearrangements they induce.

C. Simulation details

In a nutshell, given a model for the interaction forces between the different coarse-grained units forming a physical system, the technique of molecular dynamics simulation [55] provide effective methods to numerically integrate the equation of motion, conforming to different statistical ensembles and macroscopic external conditions. It has been utilized for some decades now, to explore structural and dynamical properties of complex systems and it has been shown to perform quite successfully also in the case of polymer systems [28, 56, 57] of interest here.

In what follows we express all quantities in dimensionless reduced units: length, energy and time-units are σ , ϵ and $(m\sigma^2/\epsilon)^{1/2}$, respectively [55]. All the monomers have the same mass $m = 1$. In order to give an idea of typical realistic orders of magnitude, we can associate these dimensionless quantities to reasonable values for the experimentally measured counterparts [58]. We consider as a typical unit of energy, $2k_B T$. The typical lengths are measured in units of 0.4 nm, which gives a typical order of magnitude for forces of 20 pN at ambient temperature $T = 300$ K.

Concretely, we integrated Eqs. (1) numerically using Ermak's algorithm [55, 59], with an integration time step $\delta t = 0.001$ and a friction coefficient $\xi = 10$. This technique produces realistic configurations of the system, characterized by probability distributions conforming to the canonic NVT ensemble. We calculated statistical averages over several independent instances of the dynamics and we indicate them with angular brackets, $\langle \dots \rangle$. We used a cubic simulation box of total volume V with periodic boundary conditions. The parameters in the interaction potentials are: $k = 9000$ (the elastic constant), $r_0 = 0.4$ (the equilibrium spring length) and $S = 1$. We simulated N_p chains formed by N_m monomers each. The total number of interaction sites is $N = N_p \times N_m$ and

the number density $\hat{\rho}$ is given by the ratio N/V . The actual values for N_m and N_p have been fixed by some preliminary runs on the passive system detailed in the next section.

III. PASSIVE SYSTEM: TUNING OF FILAMENT LENGTHS

We performed some preliminary simulations to select the best suited values of the remaining parameters, N_p and N_m in the limit in which the motors are switched off (passive system). We observe that the total number of interaction sites, N , is limited by our present computer capabilities, mainly due to the need of vast statistics. We first consider a system with $N_p = 250$ polymers (a safe trade between the need for minimizing finite size effects and available computational resources) and values for N_m ranging from 5 to 101, to select the optimal polymer size.

The wanted number density $\hat{\rho}=1$ is set by appropriately scaling the simulation box size. The target temperature, $T = 0.8$, corresponds to a safe liquid state. This choice of density and temperature has two important consequences. First, the passive system is in a liquid state characterized by relaxation times that are much shorter than the typical simulation total time scale and it is comfortably in equilibrium with its environment. Therefore, averages of quantities that depend on only one time (after preparation) are time-independent and two-time correlations depend on the time-delay between the measurement of the two observables. More precisely, the dynamics are stationary. Second, the chosen thermodynamical point is well inside the stable liquid phase for the passive system. This allows us, in the active case, to safely assign any non-conventional structural or dynamical feature to the motor activity alone and not to some “normal” effect due to the interaction with some phase boundary.

A. Collective static structure

We start by quantifying the polymer size dependence of the structure of the system. In Fig. 2 we show the static structure factor

$$S(\mathbf{q}) = N_m^{-1} N_p^{-1} \langle \rho(\mathbf{q}, t) \rho^*(\mathbf{q}, t) \rangle, \quad (5)$$

with $\rho(\mathbf{q}, t) = \sum_{i=1}^{N_m} \sum_{a=1}^{N_p} e^{i\mathbf{q} \cdot \mathbf{r}_{ia}(t)}$ the Fourier transform of the instantaneous density. $\mathbf{r}_{ia}(t)$ is the time-dependent position of monomer i in polymer a . Isotropy implies $S(\mathbf{q}) = S(q)$ and a spherical average over wave vectors of modulus q is considered. While the curve for $N_m = 5$ clearly falls away from the remaining data, the static structure depends only weakly on N_m as shown by the collapse of all curves with $N_m \geq 21$.

A detailed description of these results goes beyond the goal of this work, nevertheless we briefly discuss our findings in what follows. The $S(q)$ of Fig. 2 show the typical

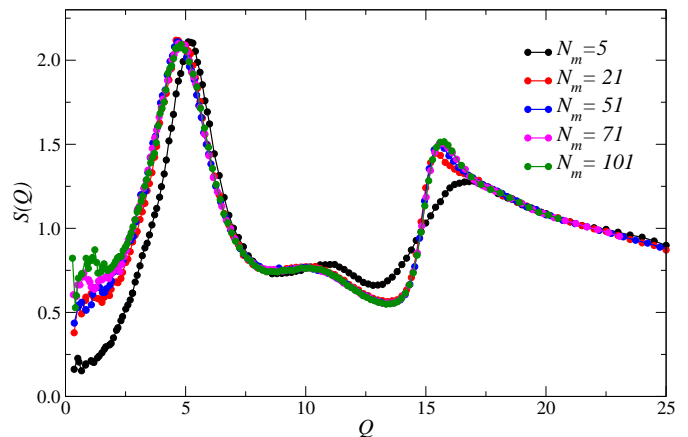


FIG. 2: Study of the passive system at $T = 0.8$ and $\hat{\rho} = 1$. The plot shows the collective static structure factor $S(q)$ for systems with $N_p = 250$ polymers with length N_m as indicated in the legend. For N_m larger than 21 no significant differences in the static structure on the entirely investigated wave-vector q -range are observed.

features of a polymer melt, namely the presence of two principal peaks. The first one is usually related to inter-chains average distance and is at $q_0 \simeq 4.8$. The length associated to this value is about 1.26 which, as we will see below, is the typical distance between monomers pertaining to nearest neighbor polymer chains. The second peak, at position $q_1 \simeq 15.7$ is associated to the equilibrium bond distance r_0 . The feature of small intensity located at about $q = 10$ is not associated to any evident length scale, being probably due to the convolution of density fluctuations of wave vectors between q_0 and q_1 . Subsequent peaks, not shown in the figure, have less intensity reflecting the loss of spatial correlation in the liquid [60].

We note that the general shape of our curve is very similar to the one found in a united atoms model of 1,4-polybutadiene (see Ref. [56] and references therein). In contrast, and as expected, $S(q)$ is quite different from the one for highly flexible polymers modeled by a bond-spring model with Lennard-Jones interactions complemented by the finitely extensible non-linear elastic potential [61].

From this preliminary analysis $N_m = 21$ appears as the minimal polymer length to be chosen to avoid any important dependence of the collective structure on the size of the polymer.

B. Single polymer structure

An equivalent characterization of the static structure of the passive system is based on the study of the pair distribution function $g(r) = V/n^2 \langle \sum_{\alpha=1}^n \sum_{\beta \neq \alpha} \delta(r - r_{\alpha\beta}) \rangle$ with different choices of the sum ranges. This allows one to disentangle the inter and intra polymer correlations, as

shown in Fig. 3 for the case $N_p = 250$ and $N_m = 21$. Data in panel a) are calculated summing over all monomers in the system; data in panels b) and c), instead, correspond to the sums performed over monomers pertaining to different polymers and monomers pertaining to the same chain, respectively. Data in a) are the convolution of the curves shown in b) and c). These results give additional support to the description proposed in Sect. III A.

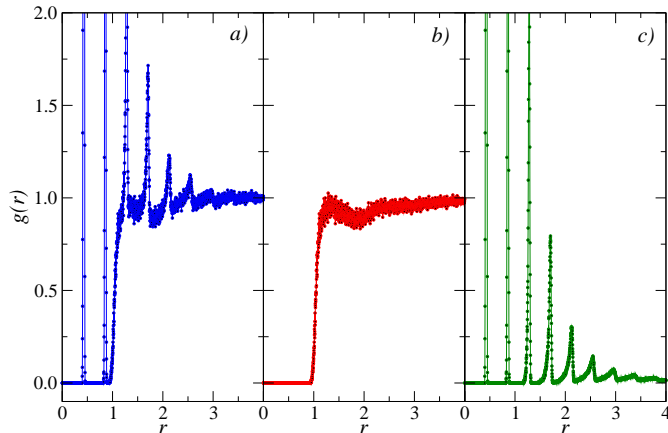


FIG. 3: Study of the passive system at $T = 0.8$ and $\hat{\rho} = 1$ with $N_p = 250$ and $N_m = 21$. The pair distribution functions are computed summing over a) all beads in the system; b) beads pertaining to different polymers; c) beads pertaining to the same polymer.

The analysis of the fluctuating radius of gyration [49] averaged over all polymers

$$R_g^2(t) = \left\langle \frac{1}{N_p} \sum_{a=1}^{N_p} \frac{1}{2N_m^2} \sum_{i \neq j} |\mathbf{r}_{ia}(t) - \mathbf{r}_{ja}(t)|^2 \right\rangle, \quad (6)$$

confirms that the semi-flexible chains in the melt are non-Gaussian, in opposition to what is predicted by the standard completely flexible polymer theory [49, 50]. This is shown in Fig. 9 b), again for the case $N_m = 21$, where we plot the distribution of the radius of gyration for passive and active systems. The average value for the passive system, corresponding to $R_g \simeq 2.54$ [Fig. 9 a)], has to be compared with the Gaussian model value, $R_g = r_0 \sqrt{N_m/6} \simeq 0.75$.

C. Equilibrium dynamics

The question of the role played by rigidity in the dynamics of a concentrated melt of linear polymers is highly non-trivial (see, among others, Ref. [62]) and a comprehensive study of this issue goes far beyond our present interests. Here we are primarily interested in a qualitative characterization of the self dynamics of the passive polymer system. In particular, we need to check if the value $N_m = 21$ which appears to be the best choice for

a set of $N_p = 250$ interacting filaments is characterized by a structural dynamics taking place on reasonable time scales. Our main results are summarized in Figs. 4 and 5.

In Fig. 4 a) we show the averaged (three-dimensional) mean-squared displacements

$$\Delta^2(t) = \frac{1}{N} \left\langle \sum_{a=1}^{N_p} \sum_{i=1}^{N_m} |\mathbf{r}_{ia}(t) - \mathbf{r}_{ia}(0)|^2 \right\rangle, \quad (7)$$

and in panel b) we show the self-intermediate scattering functions

$$F_s(q, t) = \frac{1}{N} \left\langle \sum_{a=1}^{N_p} \sum_{i=1}^{N_m} e^{i\mathbf{q} \cdot [\mathbf{r}_{ia}(t) - \mathbf{r}_{ia}(0)]} \right\rangle, \quad (8)$$

at $q = 4.8$, the wave-vector of the first diffraction peak in the static structure factor, in both cases calculated considering all beads and as a function of t . The chain lengths are indicated in the figure. Our data are consistent, as expected, with a picture where the larger the polymer size, the slower the relaxation. We also note that these data show the typical signatures of a liquid state, with no dynamical arrest nor crystallization.

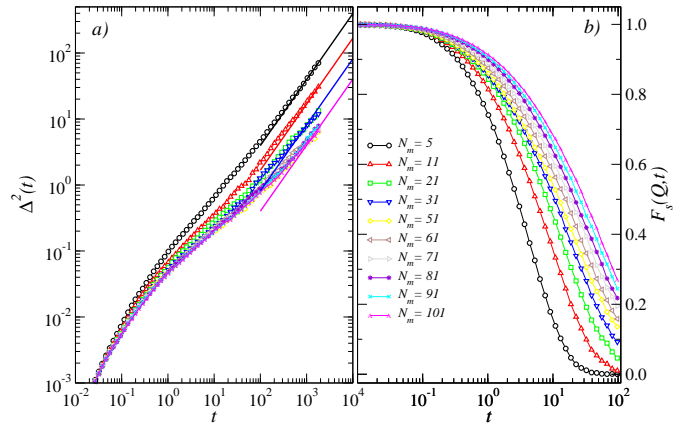


FIG. 4: a) Mean-square displacement and b) self intermediate scattering function in the passive system with $\hat{\rho} = 1$ at $T = 0.8$ as a function of t for different values of N_m given in the legend of panel b). In all cases $N_p = 250$ and all monomers have been taken into account. The limited time range used still allows for the determination of a self diffusion coefficient from a linear fit of the long time part of the mean squared displacement. Some examples are shown with solid lines. The self intermediate correlation function is calculated at a value of $q = 4.8$ corresponding to the first diffraction peak of the static structure factor.

The mean-square displacement in Fig. 4 a), presents the typical bending separating short time-scales ($t \lesssim 10^{-1}$) with ballistic motion from long time-scales ($t \gtrsim 10^{-1}$) with, at least for short chains, diffusive behavior. Indeed, although the investigated time range is quite limited, for $N_m \leq N_m^* = 50$ we can estimate a diffusion coefficient from the Einstein relation $D = \Delta^2(t)/6t$ in the

limit $t \rightarrow \infty$. These data are shown in Fig. 5 a), and points for $N_m \leq N_m^*$ are consistent with a power law N_m^{-1} (dashed line). Data for $N_m > N_m^*$ are much less convincing, saturating at a constant value. This is possibly due to the limited time scale reached, which does not actually allow us to discriminate between a diffusive behavior and a Rouse-like behavior $\propto t^{0.61}$ [28, 49, 50] which should be a signature of limited entanglement.

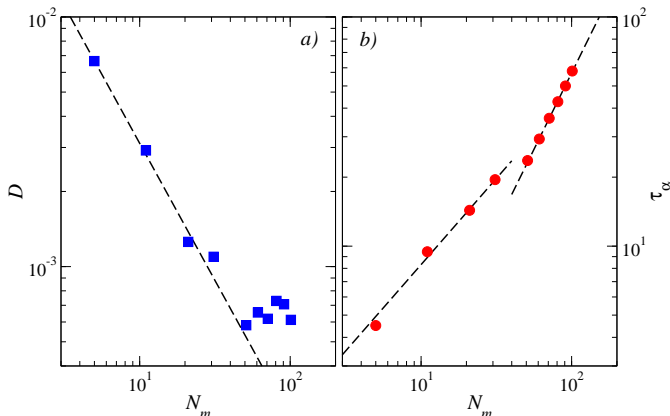


FIG. 5: a) Self diffusion coefficient D calculated by a linear fit of the long time linear behavior of the mean squared displacement, as explained in the text. The dashed line is a guide-to-the-eye. b) The relaxation time extracted from $F_s(q, t)$ for $q=4.8$ as described in the text. Note the apparent dynamical crossover at $N_m \simeq 50$. We remind that all quantities are calculated from all monomer coordinates, as discussed in the text.

The quality of our data for the intermediate scattering functions [Fig. 4 b)] allows us to extract quite comfortably an estimate for the structural relaxation time τ_α by using the model independent definition $F_s(q, \tau_\alpha) = 1/e$. Our results are shown in Fig. 5 b). We find evidence for a dynamical crossover similar to the Rouse-like to reptation-like one [50]. More precisely, we find a relaxation time $\tau_\alpha \simeq N_m^{3/4}$ for $N_m < N_m^*$ and $\tau_\alpha \simeq N_m^{4/3}$ for $N_m > N_m^*$, with $N_m^* \simeq 50$. We tentatively associate the anomalous power-law dependencies to the fact that we are dealing with semi-flexible polymers. The wave-vector dependence of τ_α is the usual hydrodynamic behavior $\tau_\alpha \simeq q^{-2}$ (not shown).

We conclude our brief study of the chain-length dependence of the structure and dynamics of a passive semi-flexible polymer melt by stating that, surprisingly enough, to the best of our knowledge, this problem has not been fully investigated in the past. The N_m^{-1} dependence of the self-diffusion coefficient is a known scaling law of quite generic polymer dynamics but we know of no previous numerical studies to compare with concerning the N_m dependence of τ_α . A complete characterization of a possible dynamical crossover corresponding to a particular chain size is also lacking. All these matters are of limited interest in the context of the study of T_{eff} but call for further work. Here we conclude by fixing the final

parameter $N_m = 21$ corresponding to a passive system with quite standard structural and dynamical features, taking place on time scales comfortably reachable in numerical experiments.

IV. ACTIVE SYSTEM: THE EFFECT OF MOTOR ACTIVITY

We now turn to the investigation of the structure and dynamics of the active semi-flexible polymer melt in which motors are switched on. We stress here that external macroscopic conditions are fixed and the only control parameter is the motor activity. We recall that we quantify the motor activity via a single parameter $f \equiv f^M/\bar{F}$, *i.e.*, the ratio (in the range $0.1 \div 1$) between the force exerted by the motor and the mean mechanical force, $\bar{F} \simeq 163.5$, acting on the equivalent passive system. We fix the activation motor time as $\tau = 500$ molecular dynamics steps. Similar to the inactive case detailed in Section III, we consider $N_p = 250$ polymers with $N_m = 21$ monomers each, for a total of $N = 5250$ interaction sites.

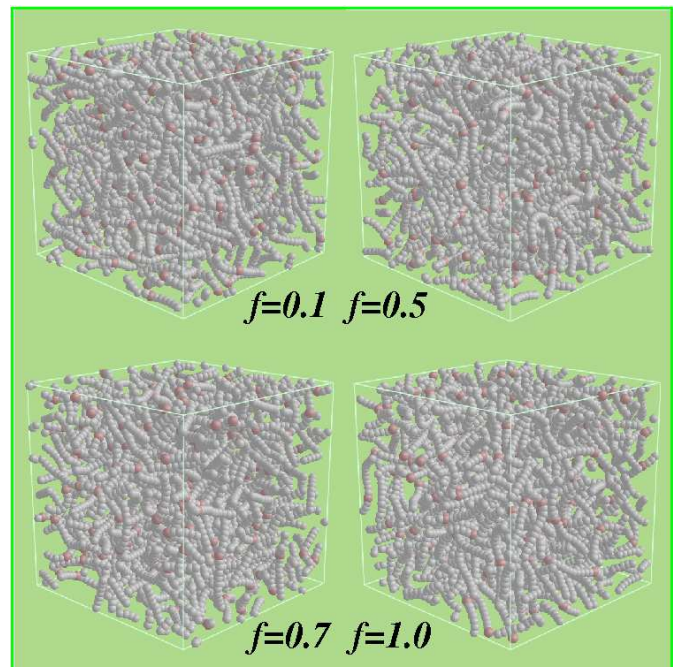


FIG. 6: Typical snapshots of the system of motorized filaments at the indicated values of the motor activity, f . Brown beads indicate the instantaneous positions of the molecular motors.

In Fig. 6 we show typical snapshots of the system produced following the above prescriptions, at the indicated values of motor activity. Differences are not immediately evident and we need to characterize quantitatively the effect of motors on intramolecular and intermolecular structure.

A. Thermodynamics

We start by analyzing the f -dependence of a few thermodynamic observables. Figure 7 presents the f dependence of the inter-molecular and intra-molecular energy, see Eqs. (3) and (4) respectively, as well as the pressure defined through the usual virial relation $PV = NT + 1/3 \langle \sum_{ia} \mathbf{r}_{ia} \cdot \mathbf{f}_{ia} \rangle$ [55]. The three quantities increase

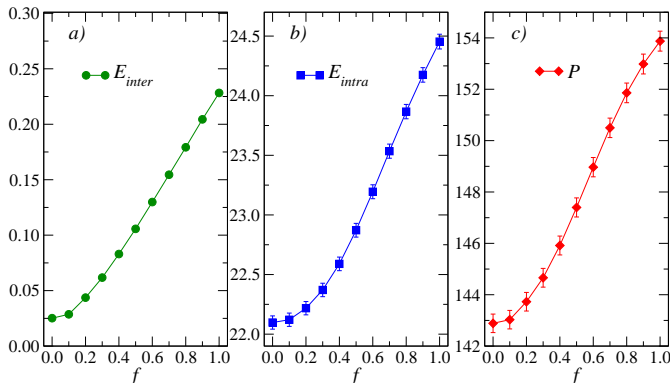


FIG. 7: Thermodynamical observables for the active system, as a function of the motor activity f defined in the text. From left to right we show the inter-molecular repulsive Lennard-Jones contribution a), the (total) intra-molecular energy b) and the total pressure c) (defined in Eqs. (3) and (4) and calculated from the usual virial relation, respectively).

smoothly for moderate forces, $f \lesssim 0.2$, next they cross over to an approximately linear, in the case of U_{inter} , and sigmoidal, in the cases of U_{intra} and P , shape. We note that the overall variation of the intermolecular potential energy is of order 8, while it is of order 0.1 for intramolecular (sum of the repulsive Lennard Jones and bonding) energy and total pressure. We also note that for the latter only the configurational term plays a role, being T constant. The results of panel a) seem to suggest a picture where distances between beads pertaining to different filaments decrease with increasing f , therefore indicating crowding.

The pressure results are also very interesting. Indeed, pressure is related to the (negative) diagonal components of the stress tensor. Thus we can anticipate that motor activity has a non-trivial effect on the mechanical properties of the filaments. This is actually what is observed in real systems, see *e.g.* Ref. [63]. Already at the level of simple thermodynamic quantities related to configurational properties motor activity is non negligible and we expect to find sensible implications on the static structure as well.

B. Collective structure

In this section we consider the static structure factor $S(q)$, see Eq. (5), and the gyration ratio defined in Eq. (6)

and we try to give a consistent picture of the motor activity effect on the static structure of the system.

In Fig. 8 we show the static structure factor as a function of motor activity. All curves have been shifted by a fixed amount for clarity, f increases from bottom to top. The general features of the structure factor are not altered by the action of the motors but, upon careful inspection, one observes some subtle changes.

Upon increasing the strength of the motor activity, the main peak position shifts to higher values of q , meaning that the average nearest neighbor distance between beads pertaining to different polymers decreases (recall that the first and highest peak is mainly determined by interchain correlations). This is also consistent with the crowding picture suggested from the study of the thermodynamic quantities in Sect. IV A. The width of the first peak increases while its height decreases with increasing f . This trend is similar to the one that one finds when increasing the bath temperature in a passive polymer liquid, see for instance the simulations in [61]. The motors have then the mixed effect of making the melt more compact and more disordered simultaneously.

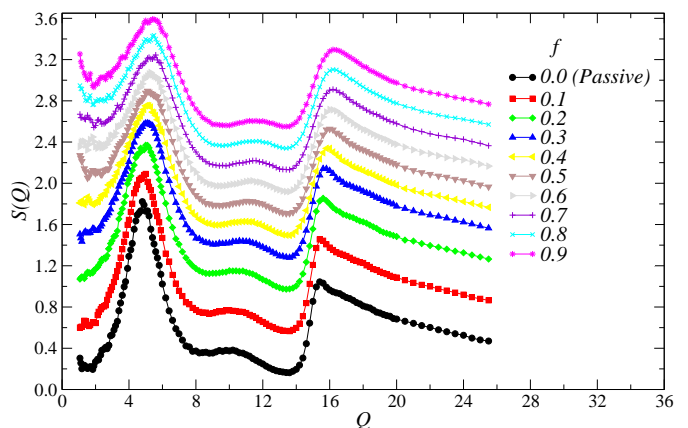


FIG. 8: Static structure factor in the active sample at the investigated motor activities parametrized by f (highest f on top). Data have been shifted vertically for clarity. The first diffraction peak increases with f as described in the text.

The second and third peaks in $S(q)$ follow the same trend, see Fig. 8, suggesting that the effect of motor activity is to fold the chains. This is consistent with the fact that the radius of gyration decreases with increasing f , see Fig. 9 a).

Working in real space one corroborates this picture. Not much information can be extracted by simply looking at the system snapshots of Fig. 6. In particular, the fact that increasing f has a sensible influence on the gyration ratio of the filaments is not evident from the snapshots, as it is when we quantify the analysis in Fig. 9. We show in Fig. 9 a) the average value of the gyration ratio as a function of motor activity. It decreases from 2.54 for the passive system to 1.7 for $f = 1$.

The probability distribution of R_g [Fig. 9 b)] suggests

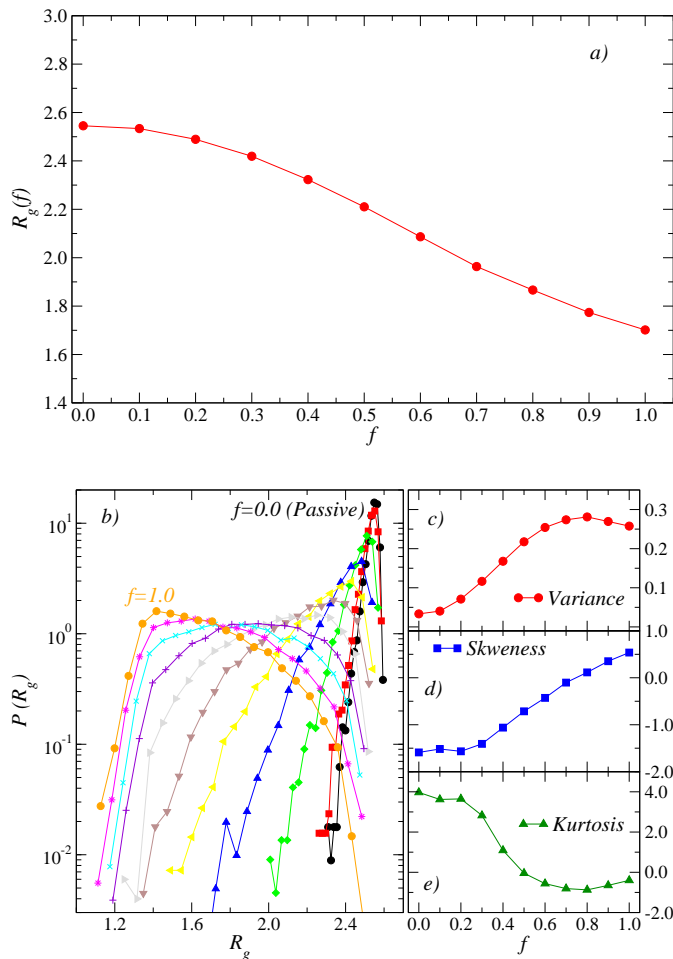


FIG. 9: a) Averaged gyration ratio. b) Probability distributions of the gyration radius at all investigated motor activities. The structure is highly non-trivial with an average value shifting towards lower values for increasing f . A more precise characterization of the distribution is given by its variance c), skewness d) and kurtosis e).

an even more complex scenario. In the passive system it is non-Gaussian and very asymmetric. We can characterize these curves very precisely with the variance, skewness and kurtosis [64] dependence on f , as shown in Fig. 9 c)-e). A cross-over between regions of different curvature is evident, but we are not in the position to justify this complex behavior. It would be very interesting to compare these data to analogous experimental measurements using scattering techniques.

In conclusion, motor activity apparently has the effect of pushing closer the filaments, which at the same time fold substantially. There is a competition between two effects: crowding, which is related to excluded volume effects and tends to slow down the dynamics; and folding of the chains, which dynamically lifts the topological constraints, therefore decreasing entanglement. This must have important consequences on the long-time evolution of our system, as we will see in the next section.

C. Dynamics

In this section we quantify the effect of motor activity on the dynamics and we compare it to the relaxation in the passive limit. We stress again that we work at constant volume and temperature, which means that all observed differences in the dynamical behavior are only due to the motor effects which are in any case chosen to be mild.

Figures 10 and 11 (main panel) display the mean-square displacement, Eq. (7), and the self-intermediate scattering function, Eq. (8) – for the wave-vector $q_0 \simeq 4.8$ of the main peak in $S(q)$ in the passive case – as a function of time-delay for all investigated motor forces given in the key. The time range considered is quite extended and allows us to comfortably reach the diffusive regime of the global displacement in which the self-intermediate scattering functions safely decay to zero.

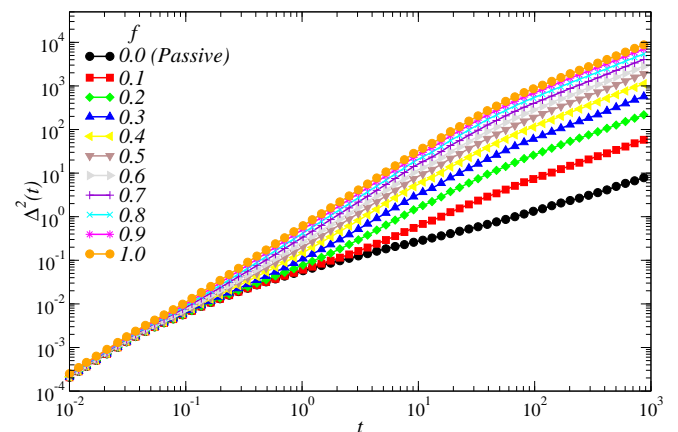


FIG. 10: Mean-squared displacement in the active system with the motor activities given in the key (higher activities on top).

Qualitatively, the data resemble the ones found in the passive system, see Fig. 4, but depend now on the motor strength. All the data are compatible with a picture where the collective dynamics of filaments gets faster under stronger motors. This is also consistent with our results on the gyration ratio and supports our interpretation: the augmented folding of the filaments seems to solve local topological constraints and diminishes the effect of entanglement.

Additional interesting information is included in the data of Fig. 11. Solid lines are best fit of our data to a curve of the form $\exp -(t/\tau)^\beta$. Values for the β coefficient as a function of f are included in the inset. Data increases with f , implying that the relaxation crosses over from stretched exponential ($\beta \leq 1$) to compressed exponential ($\beta > 1$). This unusual shape for the intermediate scattering function has been already observed in soft matter systems, like colloidal gels, emulsions or Laponite suspensions, as surveyed in a number of reviews, see, *e.g.*, Ref. [65]. In these references, the cross over is related to

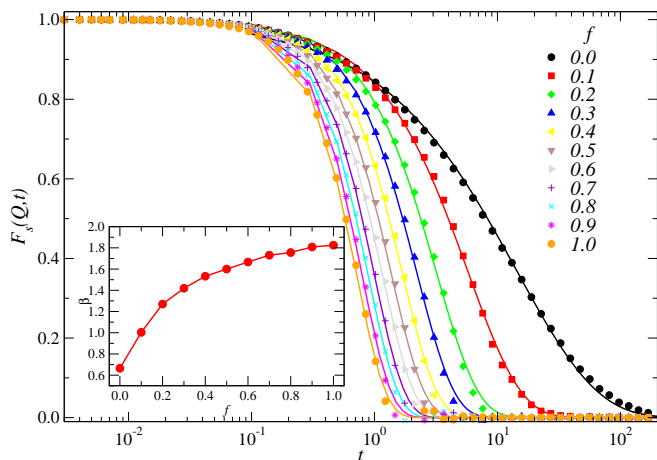


FIG. 11: Main panel: Time-dependence of the intermediate scattering functions at the wave-vector corresponding to the first maximum of the static structure factor at the investigated motor activities (activities increase to the left). Inset: values of the exponential parameter β estimated from a fit of the data to the form $\exp -(t/\tau)^\beta$ (see text for details).

randomly distributed internal stress sources acting on the sample. It is tempting to associate this sources to motor activity but, again, it is difficult to address this subject here.

An even more quantitative analysis is presented in Fig. 12, in which the dependence of the diffusion coefficient and the (inverse) relaxation time (estimated by the fit detailed above) on the strength of the motors is analyzed. Data are shown renormalized to the value of the passive system. It is very interesting to note that both sets of data are consistent with two very simple functional forms (solid lines in the figure), $D/D_{f=0} \simeq 1 + 1423 \times f^{2.29}$ and $(\tau/\tau_{f=0})^{-1} \simeq 1 + 19 \times f$, respectively. Note the extremely large variation of the diffusion coefficient that extends over three decades, and the less pronounced variation of the inverse relaxation time.

An observation is in order at this point. The f -dependence of the diffusion coefficient is reminiscent of the findings discussed in Refs. [41] and [66]. For the active colloidal particles used in these studies the effective diffusion coefficient can be written as $D = D_o + 1/3 v^2 \tau_R$, where $D_o \equiv D_{f=0} = k_B T / (6\pi\eta R)$ is the diffusion coefficient of the passive system, v is the velocity of the particle and $\tau_R = 8\pi\eta R^3 / (k_B T)$ is the rotational relaxation time. R and η are the typical radius of the colloidal particle and the viscosity of the solvent, respectively. This relation can also be written as $D/D_o = (1 + 1/9 P_e^2)$, where P_e is the Peclet number, defined as $P_e = vR/D_o$ and characterizes the particle activity [41, 67].

In our case the exponent (2.3 ± 0.1) is close to 2. The difference could be ascribed to the uncertainties in the determination of D or to the presence of corrections to the correct scaling. It is tempting to imagine that f is in this case playing the role of the Peclet number. We will

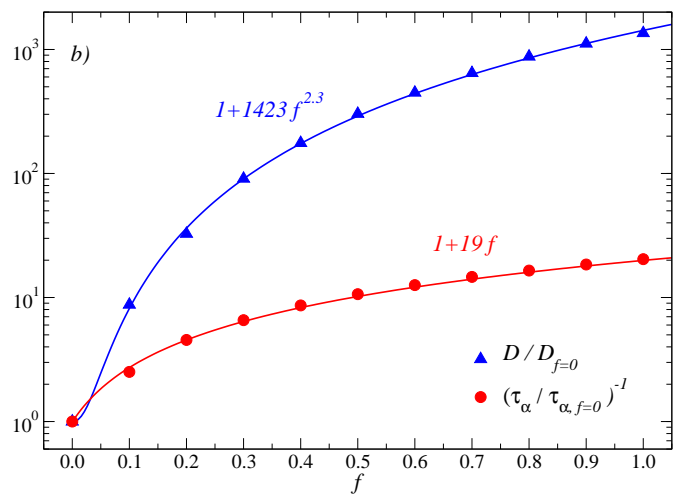


FIG. 12: Diffusion coefficient D and structural (self-)relaxation time τ as a function of f . The relaxation time values have been estimated from a fit of the data to the form $\exp -(t/\tau)^\beta$ (see text for details). The data follow power laws with exponents indicated in the figure.

see in our final discussion that this idea is indeed reasonable and our results on the effective temperature and analogous experimental data [41] seem to be compatible with the conjecture.

We have not been able to find a rationale for the linear dependence of the inverse of the relaxation time, which is also a quite striking result.

V. EFFECTIVE TEMPERATURE(S) IN COMPLEX ACTIVE MATTER

The analysis above proved that both structure and dynamics of the active system are influenced by motor activity in a very complex fashion. We ask now whether it is possible to embed all this complexity in a single parameter, also prone to be directly determined in experiments. The chosen parameter is the effective temperature T_{eff} a quantity already well characterized in different contexts, as we have discussed in the introduction [30].

In equilibrium, a model independent relation exists between the linear response of an observable, say A , to a perturbation applied to the system and the correlation between the same observable and the one that “receives” the perturbation, say B . This is the fluctuation-dissipation theorem (FDT) that reads

$$\chi_{AB}(t_1, t_2) = \frac{1}{T} [C_{AB}(t_1, t_1) - C_{AB}(t_1, t_2)], \quad (9)$$

where

$$\begin{aligned} \chi_{AB}(t_1, t_2) &= \int_{t_2}^{t_1} dt' \left. \frac{\delta \langle A(t_1) \rangle_h}{\delta h_B(t')} \right|_{h_B=0}, \\ C_{AB}(t_1, t_2) &= \langle A(t_1) B(t_2) \rangle, \end{aligned} \quad (10)$$

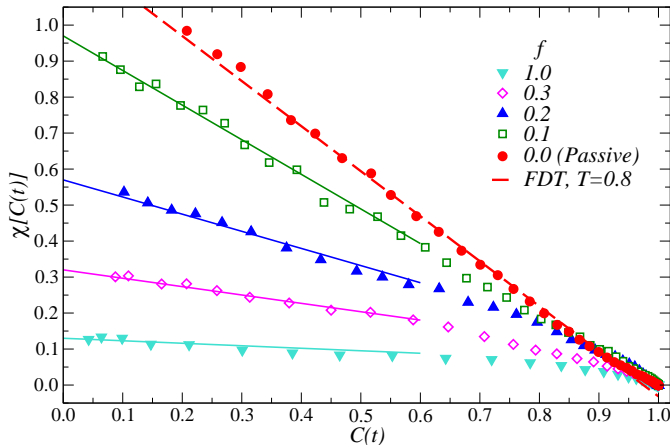


FIG. 13: Fluctuation-Dissipation relations in the motorized polymer melt. The red data on top correspond to the passive system. Solid lines are linear fits used to estimate the value of the effective temperatures. The dashed (red) line has slope $-1/T$, thus confirming the validity of the FDT at equilibrium for the passive system.

and the perturbation is such that $H \rightarrow H - h_B B$. The prefactor T^{-1} is the inverse of the temperature of the bath with which the system is in contact. In equilibrium $C_{AB}(t_1, t_1)$ is a constant, both $\chi_{AB}(t_1, t_2)$ and $C_{AB}(t_1, t_2)$ are just functions of the time difference $t = t_1 - t_2$, and Eq. (9) becomes

$$\chi_{AB}(t) = \frac{1}{T} [C_{AB}(0) - C_{AB}(t)], \quad (11)$$

for $t > 0$. In the frequency domain the FDT reads $2T\Im R_{AB}(\nu) = \nu C_{AB}(\nu)$ with the sign convention for the Fourier transform such that $R_{AB}(\nu) = \int_{-\infty}^{\infty} dt e^{i\nu t} R_{AB}(t)$.

A. Correlation-response parametric plot

One way of measuring the effective temperature in a non-equilibrium steady state consists in using the parametric relation between the out-of-equilibrium integrated linear response, $\chi_{AB}(t)$, and the correlation of a chosen pair of observables, $C_{AB}(t)$, and associating minus its inverse slope with a possibly time-dependent parameter $T_{eff}(t)$ [29, 30]:

$$\chi_{AB}(t) = \frac{1}{T_{eff}(t)} [C_{AB}(0) - C_{AB}(t)]. \quad (12)$$

Such measurements were performed in different *aging*, that is to say non-stationary, glassy systems (for details see [68]) and in out of equilibrium steady states (see, among others, Refs. [69–71]) demonstrating that $T_{eff}(t)$ is piecewise constant taking, typically, two values: the one of the environmental bath at short time-delays and

another one characterizing the structural relaxation at long time-delays.

In interacting particle problems [69] it is customary to use $A(t) = 1/N \sum_{i=1}^N \epsilon_i e^{i\vec{q} \cdot \vec{r}_i(t)}$, and $B(t) = 2 \sum_{i=1}^N \epsilon_i \cos[\vec{q} \cdot \vec{r}_i(t)]$, where the field $\epsilon_i = \pm 1$ with probability a half. With this choice the relevant equilibrium correlation function is the intermediate scattering function of Eq. (8) once the results are averaged over many instances of the ϵ_i . We have also used these observables with $q = q_0$ and we averaged over 10^2 independent field realizations.

We performed these measurements for different values of the forcing f and the results are shown in Fig. 13 in the form of the parametric plot $\chi(t)$ against $C(t)$. The curves clearly show two regimes with a relatively smooth crossover between them. We do not attribute particular importance to the first regime, corresponding to small t or high frequencies, which represents the fast vibration of monomers, surrounded by their environment, before any structural relation takes place. The second regime, being the one of long t and small frequencies, is more interesting since it describes the actual structural relaxation in the sample.

In all cases, the parametric plot in this regime is rather well described by a straight line [72], implying that T_{eff} is a constant over this time-scale. In the figure the numerical data are represented with points and the lines are the result of fits to linear functions performed on the long-times part of the curves. For the passive system the construction yields a straight line with slope equal to $-1/T$, confirming that the FDT holds in this case. The active systems have decreasing absolute value of the slope for increasing forcing and will be compared to other measurements of T_{eff} below. Data from the $\chi(C)$ determination of T_{eff} are reported in Fig. 20 with open (red) squares where we also confront to other measurements as we will discuss in depth later.

B. Tracer particles

The construction detailed in the previous section is very powerful and provides us with direct unambiguous results. Indeed, it is at the same time a tool to *demonstrate* the existence of an effective temperature and an operative method to *calculate* it [69]. The method is easily exploitable in computer simulations, where the microscopic implementation of the construction does not pose particular problems. The situation is completely different in experiments, where the coupling of each (complex) unit forming the system to the perturbation field is far from obvious. This difficulty has been circumvented by considering the dynamics of *tracers* (or *intruders*) of simple geometry, *e.g.*, spheres. These objects of micrometric size are nowadays quite simple to control and manipulate by active microrheology techniques. When immersed in extended complex environments they have been demonstrated to couple to them as to an external reservoir.

Their dynamics provide a wealth of information related to the underlying matrix state. Below we discuss a few methods to implement these ideas in our simulations, based on the use of *free* and *driven* tracer particles, respectively. A typical snapshot of our filament system with embedded tracer particles is shown in Fig. 14. We have used spherical particles that, for visualization convenience, we draw with an augmented radius in the figure.

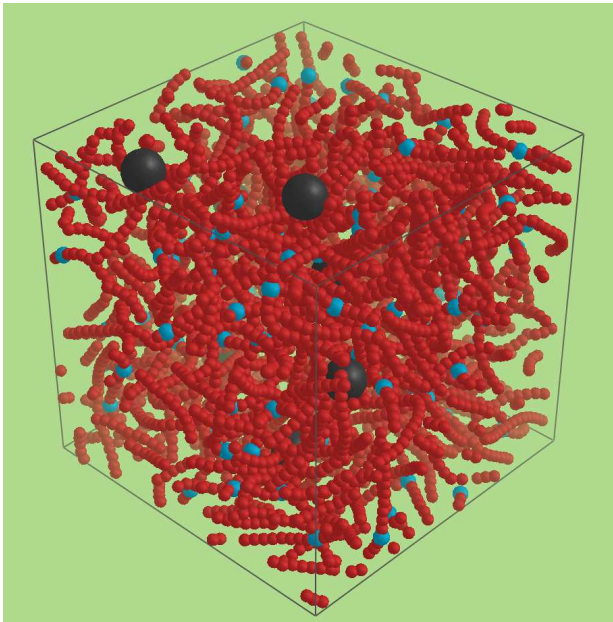


FIG. 14: Molecular dynamics computer simulation implementation of the experiment with tracer particles. We show a typical polymer configuration with 10 tracer particles; 50 per cent of polymers are motorized. Tracers have been drawn with an augmented radius for clarity.

1. Free tracers

The effective temperature should be measurable with a fine tuned thermometer that couples to the structural relaxation of the sample. A possible realization of an adapted thermometer is constituted by a *massive* – *i.e.*, of mass much larger than the mass of the polymer beads – free tracer particle immersed in the system. Indeed, it is possible to show that the kinetic energy of the tracer can be related to the system’s effective temperature via an equipartition theorem for slow modes. This kind of measurement were suggested in [29] and they were performed experimentally in granular matter [38], colloidal suspensions [40] and numerically in models of granular matter [71] and sheared atomic Lennard-Jones mixtures [69].

We consider $N_{tr} = 10$ tracer spherical particles of variable mass m_{tr} in the interval $[10 - 10^5]$, which interact with all monomers in the sample via the repulsive Lennard-Jones potential of Eq. (3). Tracers are not cou-

pled to any external thermal bath and their dynamical evolution is controlled by the usual Newton equations of motion that we have integrated with the velocity-Verlet method with $\delta t = 0.001$ in the NVE ensemble. The dynamics of polymer beads is still treated by a Langevin approach. Note that the tracers do not interact among themselves and the use of N_{tr} tracers allows for better statistics.

The results of our measurements for $f = 0.5$ are shown in Fig. 15. Panel a) displays the probability distributions of the tracer velocity, $p(v)$, where $v = |\mathbf{v}|$ and its dependence on the tracer’s mass. The data are shown using the scaled variables $p(v)/m_{tr}^{1/2}$ against $vm_{tr}^{1/2}$. The distributions are very close to Gaussian for all masses. The data are shown with points and the lines are fits to this functional form from which we extract an estimate for the effective temperature as a function of the tracer’s mass that we show in panel b).

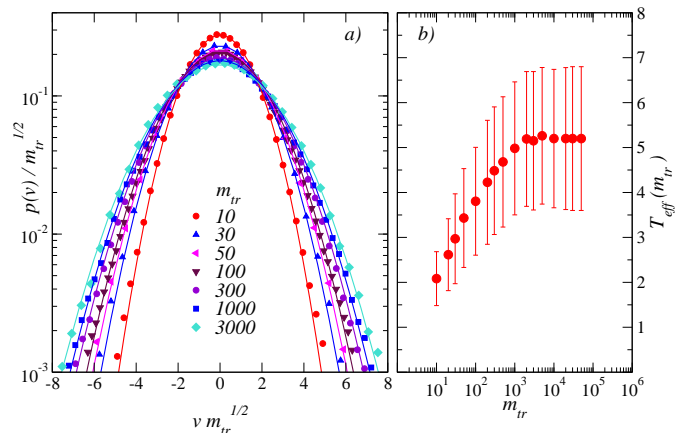


FIG. 15: a) Rescaled probability distribution of the velocities of the massive tracer particles immersed in an active sample with $f = 0.5$. The distributions are remarkably Gaussian for all tracer masses. Their variance increases with increasing mass. b) The effective temperature, extracted from a Maxwell-like fit to the distributions shown in panel a), as a function of the tracers’ mass m_{tr} .

The interpretation of these results is quite clear. Light tracers quickly react to the rapid motion of the polymers and test the short time-delay dynamics of the sample. In contrast, heavy tracers are insensitive to such rapid motion and displace themselves only due to the large-scale structural reorganization of the sample, that is to say, the long time-delay dynamics of the embedding matrix. The interesting long times – or low frequency – value of the effective temperature is then accessed in the large mass limit of this measurement.

From the figure we see that at $m_{tr} \simeq 10^3$ the variation of T_{eff} stops and the curve saturates to a constant level from which we read $T_{eff}(f = 0.5) \simeq 5.1$. Similar measurements for other values of the motors strength yield the data collected in Fig. 20 with open (blue) circles. In what follows we will consider $m_{tr} = 10^3$ which

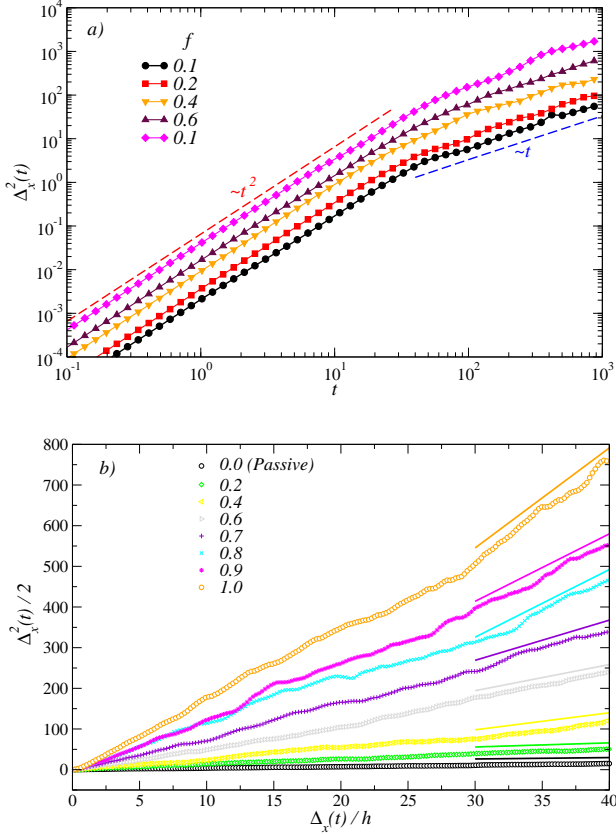


FIG. 16: a) Uni-dimensional mean-squared displacement of the free tracer particles at different values of the motor activity. b) Parametric plot of the tracer particles mean squared displacement as a function of the driven displacement, at the indicated values of motor activity. The effective temperatures have been estimated with a linear fit (solid lines) to the large mobility part of the curves.

corresponds to the smallest tracers mass coupling to the relevant slow modes of the filaments.

2. Driven tracers

Yet another independent measurement of T_{eff} is based on the use of driven tracer particles. More precisely, it is given by the study of diffusion and mobility of an ensemble of non-interacting tracer particles immersed in the active sample. These two quantities are related by the Einstein relation, one particular form of the fluctuation dissipation theorem. The (free) mean squared displacement, is the relevant equilibrium correlation function; the associated response function is the displacement induced by applying a small constant external force of intensity h to the tracer. Due to isotropy, we focus on the one dimensional version of these observables and consider the external force oriented in the \hat{x} direction.

In Fig. 16 a) we show the one dimensional free mean-square displacement for tracer particles, $\Delta_x^2(t) =$

$1/N_{tr} \langle \sum_{i=1}^{N_{tr}} (x_i^{tr}(t) - x_i^{tr}(0))^2 \rangle$, in the \hat{x} direction as a function of time-lag, for different forcing strengths given in the key. Results in the other two directions are equivalent. In all cases the tracer particles mean-square displacements cross over from ballistic motion at short time-delays to diffusive motion at longer time-delays. These two limits are shown with straight lines as guides-to-the-eye in the figure.

The one-dimensional mobility in the \hat{x} direction is calculated as $\chi_x(t) = \Delta_x(t)/(ht)$, where $\Delta_x(t) = 1/N_{tr} \langle \sum_{i=1}^{N_{tr}} (x_i^{tr}(t) - x_i^{tr}(0)) \rangle$ is the displacement calculated in independent simulations by applying to the tracers a small force $h = 0.1\bar{F}\hat{x} \simeq 16.5\hat{x}$.

Conforming to the Einstein relation $D_x/\chi_x = T$, with D_c the diffusion coefficient in the x direction and χ_x the saturated mobility, the effective temperature should also be the parameter linking the tracers' mean-square displacement and their driven displacement under a weak external applied force:

$$\frac{\Delta_x^2(t)}{2} = T_{eff} \frac{\Delta_x(t)}{h} \quad (13)$$

in the long time-lag limit in which the dynamics is diffusive. This equation is plotted in parametric form in Fig. 16 b) for the passive system and seven motor strengths given in the key. The effective temperature is given by the slope of these curves, as shown in the figure. These data are included in Fig. 20 as open (green) triangles.

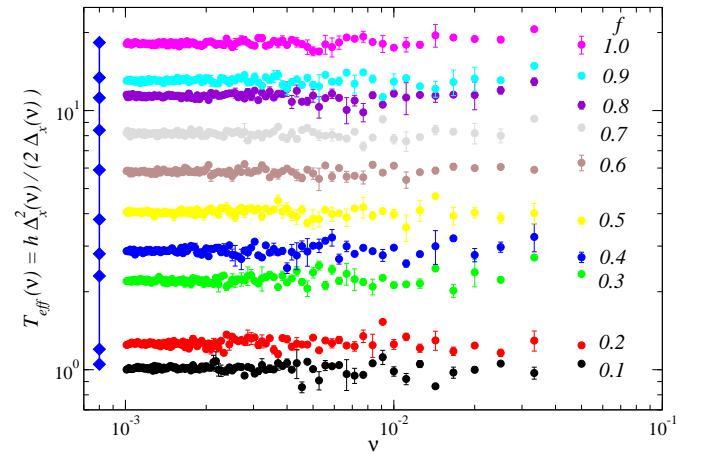


FIG. 17: The effective temperature, defined as the ratio $h\Delta_x^2(\nu)/(2\Delta_x(\nu))$, as a function of frequency. We represent as error bars the imaginary part of the ratio, to quantify the precision of the numerical Fourier transformation. Diamonds on the left are the data extracted from the linear fit shown in Fig. 16 b).

3. Frequency-dependent T_{eff} .

Parametric plots in the time-domain (Figs. 13 and 16 b)) are the standard way of identifying the values taken by the effective temperature in well-separated dynamic regimes each with a constant value of T_{eff} . They may hide, though, long crossovers in which T_{eff} does indeed depend on time. Besides, the determination of an effective temperature in experiments very often relies on measurements of spontaneous and induced fluctuations in the frequency domain.

In Fig. 17 we represent the same data shown in Fig. 16 b) in a closer way to what is implemented in experiments. We have Fourier transformed both the tracers' mean-square displacement and displacement under an external field and we present the ratio,

$$T_{eff}(\nu) = \frac{h \Delta_x^2(\nu)}{2 \Delta_x(\nu)}, \quad (14)$$

as a function of frequency. This determination of T_{eff} should coincide with the one of the time-domain in the regimes in which T_{eff} is constant. And this is indeed what we have found: for all the activation strengths and in the accessible frequency range, the curves show a relatively constant force-dependent plateau. In the limit of very low frequency we recover the frequency-independent values (diamonds) obtained by the linear fit of the parametric plot in the time-domain (Fig. 16). Although the accessible frequency range is limited by the sampling rate (upper bound) and the total time length (lower bound) of the trajectory and in principle one cannot exclude a different behavior outside this region, we conclude that no evidence of frequency dependent effective temperature has been found in the present system.

4. Free tracer dynamics.

The power of methods based on intruders has been largely demonstrated in the literature [73] and in the present work. The results contained in Fig. 18 confirm this fact and also allow one to add an interesting information: knowledge of the effective temperature dependence on f in *particular* macroscopic external conditions, *i.e.*, temperature or pressure (density), allows one to predict T_{eff} at any different macroscopic external conditions with one free tracer measure only. Indeed, we have found that a simple power law relates the diffusion coefficient of a free tracer, D , to the effective temperature characterizing the polymer matrix. All data corresponding to different temperatures or densities can be collapsed on a master curve by a simple rescaling:

$$\frac{D\rho}{T} \propto \left(\frac{T_{eff}}{T} \right)^\alpha, \quad (15)$$

with $\alpha \simeq 1$. This is exhibited in Fig. 18 where we plot the diffusion coefficients of tracer particles against

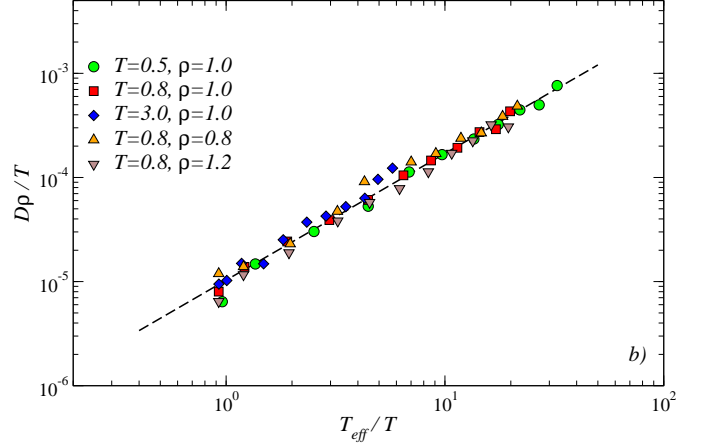


FIG. 18: Parametric plot of the rescaled diffusion coefficients for a free tracer at different values of the number density ρ and bath temperature T as a function of the rescaled effective temperatures. The dashed line is a linear fit to the data. More details are given in the text.

the effective temperature calculated by the massive particle method. This means that once the master curve is known, we can predict the value of T_{eff} by just following the free dynamics of the tracers (*i.e.*, by computing D).

We conclude this section with the following observation [74]. In the case of out-of-equilibrium glassy systems, one-time quantities converge to constants and, in particular, thermodynamic observables receive contributions from the fast regime at the ambient temperature and the slow regime at the (higher) value taken by the effective temperature, both as if they were equilibrium ones. In a sense, for these observables, the out-of-equilibrium system behaves as if it were equilibrated at T_{eff} . We could

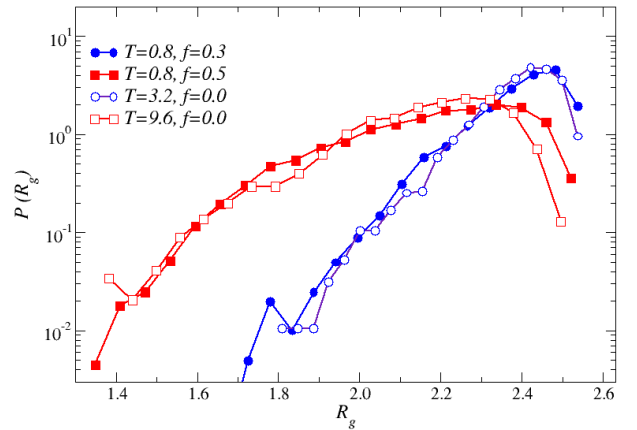


FIG. 19: Comparison between gyration radius of passive and active systems at the indicated temperatures and motor activities. See discussion in the text for details.

therefore ask, what can we say about the structure of the passive system when equilibrated at T_{eff} ? In Fig. 19 we plot the probability distributions of the radius of gyration (a one-time quantity), at the indicated values of bath temperature and motor activity. It is evident that the distributions at the higher bath temperatures for the passive case (open symbols) nicely reproduce those at $T = 0.8$ and the indicated values of activity (closed symbols). The problem is that these bath temperatures are not those we could predict from the data in Fig. 20. We believe that the connection between effective temperature and static structure is even more problematic than one could expect.

C. Survey on T_{eff} vs motor activity.

In conclusion, in this section we have shown that T_{eff} characterizes the chemical motor activity which we have schematized by the single parameter f . Figure 20 collects all our results both for self-propelled particles [43] and motorized semi-flexible filaments. The data are presented in the form T_{eff}/T against f and we also show (diamonds) average values with error bars calculated from the different determinations of T_{eff} .

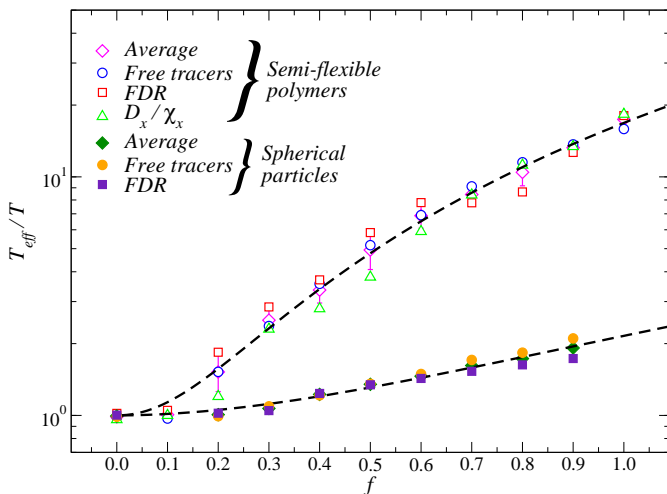


FIG. 20: This figure summarizes the entire set of data that we have generated, both for spherical self-propelled particles [43] and motorized semi-flexible polymers, on a linear-logarithmic scale. The different sets of data are indicated in the legend. Empirically, we find that all data are compatible with a power-law dependence of the effective temperature, $T_{eff}/T = 1 + \gamma f^2$ (dashed lines).

The figure demonstrates that independent determinations of T_{eff} yield consistent results suggesting that, in these systems, there is a T_{eff} parameter with a thermodynamic meaning. The data for semi-flexible lines and spherical particles fall on different curves but there was no reason for universality in this sense. They both

tend to $T_{eff} = T$ in the limit of vanishing activation, as they should, and the deviation from the environmental temperature monotonically increases with increasing forcing. The data can be fitted by the empirical law $T_{eff}/T = 1 + \gamma f^2$ with $\gamma = 15.41$ for filaments and $\gamma = 1.18$ for particles, showed with dashed lines in the figure. We note that this finding seems to support our conjecture that the parameter f plays here a role analogous to the Peclet number for colloidal active particles used in a few experiments [41], as discussed in Section IV C.

VI. CONCLUSIONS AND PERSPECTIVES

The limits of the approach used in the present work are clear. The model we have developed is quite crude and does not take into account explicitly any chemical activity nor particularly complex molecular structure. Moreover, we have chosen the most favorable conditions for producing and observing the desired effects, at the risk of perhaps being slightly unrealistic. Nonetheless, we think that our results are relevant for understanding very complex phenomena in real systems. This conviction is based on two facts.

First, our work constitutes a genuine microscopic approach to active matter. In particular, no uncontrolled hypothesis has been made, the physics of the passive system being under complete control: it conforms to previously known results and it is only due to the effect of conservative forces of very general nature. Also, the implementation of the molecular motors, the exclusive source of non equilibrium fluctuations in the system, is sufficiently general to be representative of, at least, adamant motors. In conclusion, we expect our results to be quite universal. Second, as we discuss below, our results are reminiscent of experimental findings reported in the literature. From this point of view the approach presented here can help both in rationalizing experimental observations and in suggesting new research directions.

A. Context

A number of recent publications explored fluctuation dissipation relations in biological systems or biologically motivated models. We devote the following paragraphs to the discussion of results contained in the papers that are relevant in the context of the present work.

Ziebert and Aranson [75] performed Langevin simulations of two-dimensional solutions of semi-flexible polar filaments interacting via molecular motors. They studied the rheology and structural properties in diluted samples and identified an “active temperature” T_a via a phenomenological scaling of the elastic and loss moduli. T_a increases with the average number of motors per filament and with the motor velocity. This definition is, though, not necessarily equivalent to the one that we used. Closer to our work are the following studies.

By comparing a hair bundle’s spontaneous oscillations with its response to small mechanical stimuli, Martin *et al.* [76] demonstrated the breakdown of the FDT, and thus confirmed that a hair bundle’s spontaneous movements are produced by energy-consuming elements within the hair cell.

In [63] the fluctuation-dissipation relation in a model cell system formed by three fundamental components (myosin II, actin filaments, and cross-linkers) was studied in equilibrium and out-of-equilibrium conditions. FDT holds in the former and fails in the latter situation. In these papers, the violation of FDT was used as a proof of the non-equilibrium character of the dynamics induced by molecular motors.

The effective temperature stemming from deviations from FDT has been used to study the stability of motorized particles in cytoplasm [54]. Interestingly enough, values of T_{eff} that are lower than the ambient temperature were found when considering motors that are aware of the free-energy landscape and act only in the direction of lowering its instantaneous value. The motors used in our study are not of this kind and the values of T_{eff} obtained are consistently higher than the ambient T . Such an “inversion” also occurs in cases in which the initial configuration is chosen to be to be one of equilibrium at a lower T than the working one [77].

A simple birth-death process and a general two-species interacting process, as simplified models of gene networks, were studied from the effective temperature perspective in [78]. The aim of this paper was to propose to use T_{eff} as a means to distinguish between intrinsic and extrinsic noise sources.

Morozov *et al.* [79] studied a model of the cytoskeletal network made of semi-flexible polymers subject to thermal and motor-induced fluctuations, modeled as either additive or multiplicative colored noise. They found violations of the conventional FDT leading to a T_{eff} that exceeds the thermodynamic temperature T only in the low-frequency domain where motor agitation prevails over thermal fluctuations. This is consistent with our numerical findings. However, T_{eff} in this phenomenological model is continuously frequency dependent while our data suggest that there is a low frequency regime in which it reaches a constant value, as in glassy systems.

Fluctuation-dissipation ratios were used to extract information about the degree of frustration, due to the existence of many metastable disordered states, in two self-assembly processes: the formation of viral capsids, and the crystallization of sticky discs [80].

Joly *et al.* [42] used numerical techniques to study the non-equilibrium steady state dynamics of a heated crystalline nanoparticle suspended in a fluid. A two-temperature scenario holds in this case. Indeed, by comparing the mobility to the velocity correlation function, FDT approximately holds at short-time lags with a temperature value that coincides with the kinetic one. In contrast, at long-time lags data are compatible with the temperature estimated by using the Einstein relation.

Ben-Isaac *et al.* [81] analyzed the Langevin dynamics of a single particle randomly kicked by motors as a toy model of active matter. They focused on the deviations of T_{eff} from T and the distribution of velocities from Gaussian as parameters that quantify the out of equilibrium nature of the dynamics, finding that while the former is robust the latter is not. Comparison to measurements in ATP-driven red-blood cells is also provided in this paper.

Finally, let us sum up the results in the experimental work of Palacci *et al.* [41] that is, indeed, the closest to our work. These authors investigated the effective temperature by following Perrin’s analysis of the density profile in the steady state of an active colloidal suspension under gravity. The active particles used – Janus particles – are chemically powered colloids and the suspension was studied with optical microscopy. The measurements show that the active colloids are hotter than in the passive limit with an effective temperature that increases as the square of the parameter that controls activation, the Peclet number, a dependence that is highly reminiscent of the f^2 -dependence we found with our simulations.

This summary proves that there is an increasing activity in the study of FDT violations and their interpretation in terms of effective temperatures in biophysics problems. A comprehensive experimental study of the thermodynamic properties, as we tried to present in this work within one system is, however, still lacking. In our opinion the active colloidal suspension used in [41] appears as the most suitable experimental system where to deal with this kind of questions.

B. Discussion

Let us now critically review our findings. We presented a study of active matter made of semi-flexible filaments in interaction. In the passive limit the conservative interaction parameters put the system in a liquid phase. The equilibrium polymer melt has, though, properties that are different from the ones found in the limits of completely rigid or totally flexible polymers. For example, the individual chains are not Gaussian.

Under the action of mild motor forces, the structure and dynamics are significantly modified. The analysis of the chain radius of gyration suggests that the polymers become more compact for increasing forces. This is consistent with the behavior of thermodynamic quantities that suggest crowding under increasing forces. On the other hand, the study of the static structure factors suggests that the melt gets more disordered –as in a passive sample in contact with hotter baths– and that chains become more folded when f increases. As a consequence, the dynamics gets faster under stronger forces. This is shown by the fact that the relaxation time, as extracted from the evolution of the incoherent scattering function, decreases, while the diffusion coefficient increases, for increasing f .

Next, we developed an in-depth study of the effective temperature of the active system, by using a number of independent measurements. The results of all these measurements in the semi-flexible polymer sample, as well as the outcome of similar measurements in the self-propelled point-particle model we analyzed in [43], are summarized in Fig. 20.

The dependence of T_{eff} on f conforms to our intuition. We dealt with motors that act randomly – and ignore their effect on the energy landscape of the system. They have the effect of disordering the sample and, consequently, the stronger f the higher T_{eff} . In their study of point-particle active matter [54], Shen and Wolynes argued that motors that act selectively, only when they contribute to decreasing the system’s free-energy density, lead to out of equilibrium dynamics with lower effective temperature than the environmental one. The interpretation is that this kind of motor orders the sample more than the passive system would be in equilibrium at the working bath temperature. A similar inversion has been observed in relaxing passive systems driven from an ordered initial equilibrium condition to a point in parameter space in which the evolution slowly tends to reach a less ordered final equilibrium state [77]. In this case, the dynamic configurations are also more ordered than the target equilibrium ones and, as a consequence, their effective temperature is lower than the one of the bath.

The results discussed in this paper and in Ref. [43] give a different perspective on the dynamics of active matter than the coarse-grained hydrodynamic descriptions [15–17]. While in the mode-coupling study in [16] a strong frequency dependence of the effective temperature was found, in our simulations the behavior observed is, in contrast, very similar to the one advocated in [29] to be the one of interacting glassy-like systems evolving in a small entropy production limit. Indeed, the global behav-

ior of T_{eff} in the active matter polymer system resembles the one computed in a variety of atomic models in the glassy regime [68], sheared super-cooled liquids [69], driven vortex systems [70] or even vibrated granular matter [71]. Independent measurements of T_{eff} yield consistent results in the atomic and molecular cases, as shown in Fig. 20, giving support to the idea that T_{eff} can be considered to be a thermodynamic object, at least in the weakly driven cases studied here ($f \leq 1$). It would be interesting to test whether a similar phenomenology arises in lattice models of Vicsek-type [4, 22] with various independent measurements of T_{eff} yielding the same result. On the experimental front, it would be welcome to extend the analysis of T_{eff} in the dilute active suspension of artificial swimmers studied in [41] or search for T_{eff} in artificial samples such as the ones recently designed for their tunability [82].

Finally, it would be interesting to explore the possibilities offered by the approach described in this work to clarify the extremely complex phenomenology of cell mechanical stability [8]. In particular, one could try to give an answer to the question as to how mechanical properties like elastic moduli change with motor activity and whether these changes can also be rationalized in terms of the effective temperature.

Acknowledgments

We thank J.-L. Barrat, G. Gonnella and A. Parmegiani for useful comments. This research was supported in part by the National Science Foundation under Grant No. NSF PHY05-51164.

-
- [1] D. A. Fletcher and P. L. Geissler, *Annu. Rev. Phys. Chem.* **60**, 469 (2009). G. I. Menon, arXiv:1003.2032. S. Ramaswamy, *Annu. Rev. Cond. Matt. Phys.* **1**, 323 (2010).
 - [2] C. Dombrowski, L. Cisneros, L. Chatkaew, R. E. Goldstein, and J. O. Kessler, *Phys. Rev. Lett.* **93**, 098103 (2004). E. B. Steager, C-B Kim, and M. J. Kim, *Phys. Fluids* **20**, 073601 (2008). R. Di Leonardo, L. Angelani, G. Ruocco, V. Iebba, M.P. Conte, S. Schippa, F. De Angelis, F. Mecarini, and E. Di Fabrizio, *Proc. Nac. Acad. Sc. USA* **107**, 9541 (2010).
 - [3] H. C. Berg, *Nature* **254**, 389 (1975).
 - [4] T. Vicsek, A. Czirók, E. Ben-Jacob, I. Cohen, and O. Shochet, *Phys. Rev. Lett.* **75**, 1226 (1995). E. Ben-Jacob, I. Cohen, O. Sochet, A. Tenenbaum, A. Czirók, and T. Vicsek, *Phys. Rev. Lett.* **75**, 2899 (1995).
 - [5] A. Czirók, H. E. Stanley, and T. Vicsek, *J. Phys. A* **30**, 1375 (1997).
 - [6] J. Howard, *Mechanics of motor proteins and the cytoskeleton* (Sinauer Associates Inc., 2001).
 - [7] B. Alberts, A. Johnson, J. Lewis, M. Raff, K. Roberts, and P. Walter, *The molecular biology of the cell* 4th ed. (Garland, New York, 2002).
 - [8] A. R. Bausch and K. Kroy, *Nature Physics* **2**, 231 (2006). K. E. Kasza, A. C. Rowat, J. Liu, T. E. Angelini, C. P. Brangwynne, G. H. Koenderink, and D. A. Weitz, *Current Opinion in Cell Biology* **19**, 101 (2007). D. A. Fletcher and R. Dyche Mullins, *Nature* **463**, 485 (2010). F. Jülicher, K. Kruse, J. Prost, and J.-F. Joanny, *Phys. Rep.* **449**, 3 (2007).
 - [9] F. C. MacKintosh and C. F. Schmidt, *Current Opinion in Cell Biology* **22**, 29 (2010).
 - [10] L. Deng, X. Trepate, J. P. Butler, E. Millet, K. G. Morgan, D. A. Weitz, and J. J. Fredberg, *Nature Materials* **5**, 636 (2006).
 - [11] J. Toner and Y. Tu, *Phys. Rev. E* **58**, 4828 (1998). J. Toner, Y. Tu, and S. Ramaswamy, *Ann. Phys.* **318**, 170 (2005).
 - [12] E. Ben-Jacob, I. Cohen, and H. Levine, *Adv. in Phys.* **49**, 395 (2000).

- [13] F. J. Nédélec, T. Surrey, A. C. Maggs, and S. Leibler, *Nature* **389**, 305 (1997).
- [14] T. Surrey, *Science* **292**, 1167 (2001).
- [15] K. Kruse, J.-F. Joanny, F. Jülicher, J. Prost, and K. Sekimoto, *Phys. Rev. Lett.* **92**, 078101 (2004); *Eur. Phys. J. E* **16**, 5 (2005). R. Voituriez, J.-F. Joanny, and J. Prost, *Phys. Rev. Lett.* **96**, 028102 (2006).
- [16] Y. Hatwalne, S. Ramaswamy, M. Rao, and R. A. Simha, *Phys. Rev. Lett.* **92**, 118101 (2004);
- [17] T. B. Liverpool and M. C. Marchetti, *Phys. Rev. Lett.* **90**, 138102 (2003); *Phys. Rev. Lett.* **97**, 268101 (2006).
- [18] J. Tailleur and M. E. Cates, *EPL* **86**, 60002 (2009). A. G. Thompson, J. Tailleur, M. E. Cates, and R. A. Blythe, *J. Stat. Mech.* P02029 (2011).
- [19] A. W. C. Lau and T. C. Lubensky, *Phys. Rev. E* **80**, 011917 (2009).
- [20] A. Vaziri and A. Gopinath, *Nature Materials* **7**, 15 (2008).
- [21] I. Llopis and I. Pagonabarraga, *Europhys. Lett.* **75**, 999 (2000). D. Marenduzzo, E. Orlandini, M. E. Cates, and J. M. Yeomans, *Phys. Rev. E* **76**, 031921(2007). C. M. Pooley and J. M. Yeomans, *Comp. Phys. Comm.* **179**, 159 (2008). M. E. Cates, O. Henrich, D. Marenduzzo, and K. Stratford, *Soft Matter* **5**, 3791 (2009).
- [22] H. Chaté, F. Ginelli, G. Grégoire, and F. Raynaud, *Phys. Rev. E* **77**, 046113 (2008).
- [23] G. Gonnella and G. P. Saracco, unpublished.
- [24] W. Götze, in *Liquids, Freezing and the Glass Transition*, Les Houches Session 51, 1989, ed. by D. Lesvesque, J. P. Hansen, and J. Zinn-Justin (North-Holland, Amsterdam, 1991).
- [25] L. F. Cugliandolo, in *Slow relaxation in glassy systems*, Les Houches session 77, J-L Barrat *et al* eds. (Springer, Berlin, 2003), cond-mat/0210312.
- [26] A. Cavagna, *Phys. Rep.* **51**, 476 (2009). F. Zamponi, arXiv:1008.4844. L. Berthier and G. Biroli, arXiv:1011.2578.
- [27] K. Binder and W. Kob, *Glassy materials and disordered solids* (World Scientific, 2005).
- [28] J-L Barrat, J. Baschnagel, and A. Lyulin, arXiv:1001.2065.
- [29] L. F. Cugliandolo, J. Kurchan, and L. Peliti, *Phys. Rev. E* **55**, 3898 (1997). L. F. Cugliandolo and J. Kurchan, *Physica A* **263**, 242 (1999); *J. Phys. Soc. Japan* **69**, 247 (2000).
- [30] L. F. Cugliandolo, arXiv:1104.4901.
- [31] U. M. B. Marconi, A. Puglisi, L. Rondoni, and A. Vulpiani, *Phys. Rep.* **461**, 111 (2008).
- [32] P. C. Hohenberg and B. I. Shraiman, *Physica D* **37**, 109 (1989).
- [33] P. Ilg and J.-L. Barrat, in *Statistical Physics of Ageing Phenomena and the Glass Transition Book Series*, *J. Phys. Conf. Series* **40**, 76 (2006).
- [34] T. Grigera and N. E. Israeloff, *Phys. Rev. Lett.* **83**, 5038 (1999).
- [35] D. Hérisson and M. Ocio, *Phys. Rev. Lett.* **88**, 257202 (2002). *Eur. Phys. J. B* **40**, 283 (2004).
- [36] L. Buisson, S. Ciliberto, and A. Garcimartín, *Europhys. Lett.* **63**, 603 (2003). H. Oukris and N. E. Israeloff, *Nature Physics* **6**, 135 (2010).
- [37] A. R. Abate and D. J. Durian, *Phys. Rev. Lett.* **101**, 245701 (2008).
- [38] P. Wang, C. Song, C. Briscoe, and H. A. Makse, *Phys. Rev. E* **77**, 061309 (2008).
- [39] N. Greinert, T. Wood, and P. Bartlett, *Phys. Rev. Lett.* **97**, 265702 (2006). B. Abou and F. Gallet, *Phys. Rev. Lett.* **93**, 160603 (2006). S. Jabbari-Farouji, D. Mizuno, M. Atakhorrami, F. C. MacKintosh, C. F. Schmidt, E. Eiser, G. H. Wegdam, and D. Bonn, *Phys. Rev. Lett.* **98**, 108302 (2007). P. Jop, J. R. Gomez-Solano, A. Petrosyan, and S. Ciliberto, *J. Stat. Mech.* P04012 (2009). C. Maggi, R. Di Leonardo, J. C. Dyre, and G. Ruocco, *Phys. Rev. B* **81**, 104201 (2010).
- [40] see, *e.g.*, P. Wang, C. Song, and H. A. Makse, *Nature Physics* **2**, 526 (2006) and refs. therein.
- [41] J. Palacci, C. Cottin-Bizonne, C. Ybert, and L. Bocquet, *Phys. Rev. Lett.* **105**, 088304 (2010).
- [42] L. Joly, S. Merabia, and J.-L. Barrat, arXiv:1101.2758.
- [43] D. Loi, S. Mossa, and L. F. Cugliandolo, *Phys. Rev. E* **77**, 051111 (2008).
- [44] T. A. Liverpool, *Phil. Trans. R. Soc. A* **364**, 3335 (2006).
- [45] L. Le Goff, F. Amblard, and E. M. Furst, *Phys. Rev. Lett.* **88**, 018101 (2002).
- [46] P. Bursac, G. Lenormand, B. Fabry, M. Oliver, D. A. Weitz, V. Viasnoff, J. P. Butler, and J. J. Fredberg, *Nature Materials* **4**, 557 (2005); G. Lenormand, P. Bursac, J. P. Butler, and J. J. Fredberg, *Phys. Rev. E* **76**, 041901 (2007).
- [47] I. Y. Wong, M. L. Gardel, D. R. Reichman, E. R. Weeks, M. T. Valentine, A. Bausch, and D. A. Weitz, *Phys. Rev. Lett.* **92**, 178101 (2004).
- [48] D. Loi, S. Mossa, and L. F. Cugliandolo, *Soft Matter* **7**, 3726 (2011).
- [49] P.-G. de Gennes, *Scaling concepts in polymer physics* (Cornell University Press, 1979).
- [50] M. Doi and S. F. Edwards, *The theory of polymer dynamics* (Clarendon Press, 1986).
- [51] The persistence length, λ_P , is usually defined as the characteristic length scale for the exponential decay of the two-point correlation function between unit tangent vectors along a polymer and quantifies its degree of stiffness. Only pieces of the polymer of length shorter than persistence length appear rigid and maintain an average straight conformation with a preferred tangent direction. In contrast, pieces of size larger than λ_P appear completely flexible. The contour length, λ_C , is defined as the maximum end-to-end distance of a linear polymer chain. In the present semi-flexible case the persistence length is comparable to the contour length.
- [52] D. C. Morse, *Macromolecules* **31**, 7030 (1998); *ibid.* 7044; **32**, 5934 (1998).
- [53] T. Miura, R. Kishi, M. Mikami, and Y. Tanabe, *Phys. Rev. E* **63**, 061807 (2001).
- [54] T. Shen and P. G. Wolynes, *Proc. Nac. Acad. Sc. USA* **101**, 8547 (2004); *Phys. Rev. E* **72**, 041927 (2005).
- [55] M. P. Allen and D. J. Tildesley, *Computer simulation of liquids* (Clarendon Press, 2nd ed., 1989).
- [56] W. Paul and G. D. Smith, *Rep. Prog. Phys.* **67**, 1117 (2004).
- [57] W. Paul, G. D. Smith, D. Y. Yoon, B. Farago, S. Rathgeber, A. Zirkel, L. Willner, and D. Richter, *Phys. Rev. Lett.* **80**, 2346 (1998).
- [58] D. K. Klimov and D. Thirumalai, *Proc. Nac. Acad. Sc. USA* **96**, 6166 (1999).
- [59] D. L. Ermak and J. A. McCammon, *J. Chem. Phys.* **69**, 1352 (1978).
- [60] J. P. Hansen and I. R. Mc Donald, *Theory of simple liquids* (Academic, New York, 1988).

- [61] S-H Chong, M. Aichele, H. Meyer, M. Fuchs, and J. Baschnagel, Phys. Rev. E **76**, 051806 (2007).
- [62] M. Bulacu and E. van der Giessen, Phys. Rev. E **76**, 011807 (2007); J. Chem. Phys. **123**, 114901 (2005).
- [63] D. Mizuno, C. Tardin, C. F. Schmidt, and F. C. MacKintosh, Science **315**, 370 (2007).
- [64] We recall that variance, skewness and kurtosis characterize width, asymmetry and peakedness of a probability distribution, respectively.
- [65] L. Cipelletti, and L. Ramos, J. Phys.: Condens. Matter **17**, R253 (2005). L. Cipelletti, L. Ramos, S. Manley, E. Pitard, D. A. Weitz, E. E. Pashkovski, and M. Johansson, Faraday Discuss. **123**, 237 (2003).
- [66] J. R. Howse, R. A. L. Jones, A. J. Ryan, T. Gough, R. Vafabakhsh, and R. Golestanian, Phys. Rev. Lett. **99**, 048102 (2007).
- [67] A. Baskaran and M. C. Marchetti, Proc. Natl. Acad. Sci. USA **106**, 15567 (2009).
- [68] G. Parisi, Phys. Rev. Lett. **79**, 3660 (1997). W. Kob and J-L Barrat, Eur. Phys. J B **13**, 319 (2000). R. Di Leonardo, L. Angelani, G. Parisi and G. Ruocco, Phys. Rev. Lett. **84**, 6054 (2000). L. Berthier, Phys. Rev. E **76**, 011507 (2007). S. Bustingorry, L. F. Cugliandolo, and D. Domínguez, Phys. Rev. B **75**, 024506 (2007).
- [69] L. Berthier and J-L Barrat, Phys. Rev. Lett. **89**, 95702 (2002); J. Chem. Phys. **116**, 6228 (2002).
- [70] A. B. Kolton, R. Exartier, L. F. Cugliandolo, D. Domínguez, and N. Grönbech-Jensen, Phys. Rev. Lett. **89**, 227001 (2002).
- [71] H. A. Makse and J. Kurchan, Nature **415**, 614 (2002). F. Q. Potiguar and H. A. Makse, Eur Phys J E **19**, 171 (2006).
- [72] Note that this is not the same as defining the effective temperature as the long time limit of $\chi(t)/C(0)$. As noted in Ref. [69], the latter method corresponds to determine T_{eff} as the average slope of the parametric plot, therefore neglecting the separation of time scales and finding inaccurate results [83].
- [73] see, for instance, G. Gradenigo, A. Sarracino, D. Villamaina, T. S. Grigera, and A. Puglisi, J. Stat. Mech. L12002 (2010).
- [74] We are indebted to an anonymous referee of [48] who raised our attention on this point.
- [75] F. Ziebert and I. S. Aranson, Phys. Rev. E **77**, 011918 (2008).
- [76] P. Martin, A. Hudspeth, and F. Jülicher, Proc. Nat. Acad. Sc. USA **98**, 14380 (2001).
- [77] L. Berthier, P. W. Holdsworth, and M. Sellitto, J. Phys. A **34**, 1805 (2001). J. L. Iguain, S. Bustingorry, and L. F. Cugliandolo, J. Stat. Mech. P09008 (2007). J. L. Iguain, S. Bustingorry, A. B. Kolton, and L. F. Cugliandolo, Phys. Rev. B **80**, 094201 (2009). P. Calabrese, A. Gambassi, and F. Krzakala, J. Stat. Mech. P06016 (2006).
- [78] T. Lu, J. Hasty, and P. G. Wolynes, Biophys. J. **91**, 84 (2006).
- [79] K. I. Morozov and L. M. Pismen, Phys. Rev. E **81**, 061922 (2010).
- [80] R. L. Jack, M. F. Hagan, and D. Chandler, Phys Rev E **76**, 021119 (2007).
- [81] E. Ben-Isaac, Y. Park, G. Popescu, F. L. H. Brown, N. S. Gov, and Y. Shokef, arXiv:1102.4508.
- [82] J. Deseigne, O. Dauchot, and H. Chaté, Phys. Rev. Lett. **105**, 098001 (2010).
- [83] I. K. Ono, C. S. O'Hern, S. A. Langer, A. J. Liu, and S. R. Nagel, Phys. Rev. Lett. **89**, 095703 (2002).